



Synthesis, characterization and molecular structure of Ru(II) complex with benzoylpyrazine carboxylic acid derivatives

J.G. Małecki^{a,*}, A. Maroń^a, M. Serda^b, M. Dolezal^c, J. Polański^b

^a Department of Crystallography, Institute of Chemistry, University of Silesia, 9th Szkolna St., 40-006 Katowice, Poland

^b Department of Organic Chemistry, Institute of Chemistry, University of Silesia, 9th Szkolna St., 40-006 Katowice, Poland

^c Department of Pharmaceutical Chemistry and Drug Control, Charles University in Prague, Faculty of Pharmacy, 500-05 Hradec Králové, Czech Republic

ARTICLE INFO

Article history:

Received 30 March 2012

Accepted 25 April 2012

Available online 7 May 2012

Keywords:

Pyrazines

Ruthenium(II) hydride carbonyl complexes

X-ray structure

UV–Vis

Luminescence

DFT

TD-DFT

ABSTRACT

Two benzoylpyrazine ligands containing carboxyl and amide functions and their hydride-carbonyl complexes of ruthenium were synthesized and characterized by infrared, proton, carbon phosphorus nuclear magnetic resonance, electronic absorption and emission spectroscopy and X-ray crystallography. The experimental studies were completed by theoretical calculations. From the electronic spectrum of the complex the Racah's and nephelauxetic parameters are calculated. The electronic structure of the complexes, presented in particular by the density of states diagram, have been correlated with its ability to fluoresce and used to analyze the UV–Vis spectra.

© 2012 Elsevier Ltd. All rights reserved.

1. Introduction

Pyrazine is crucial biomolecule which possess excellent coordination properties as convenient *N*-donor ligand [1,2]. Moreover the structure of pyrazine can be considered as a privileged structure which occurs in many bioactive compounds [3,4]. For example pyrazinamide (PZA), an analogue of nicotinamide, is a unique common used anti-tuberculosis prodrug which is activated to active form in acid conditions. Dolezal et al. described [5,6] antifungal and antimycobacterial properties of selected benzoylpyrazines and their derivatives. Thus the investigation of pyrazine ruthenium complexes could be interesting due to their potential applications in drug development.

On the other hand the ruthenium hydride complexes containing carbonyl and triarylphosphine ligands are interesting due to their reactivity and efficiency as catalysts in wide spectrum of reactions [7–12]. The studies on synthesis and characterization of ruthenium complexes containing nitrogen heteroaromatic ligands have received considerable recent attention, owing to their interesting photophysical and photochemical properties. Pyrazine, its derivatives as well as other 1,4-diazines, i.e. compounds with partial pyrazine structure (e.g. quinoxaline, phenazine, pteridine, flavin and their derivatives), demonstrate unique physico-chemical

properties that are caused by a low lying unoccupied π -molecular orbital and by the ability to act as a bridging ligand.

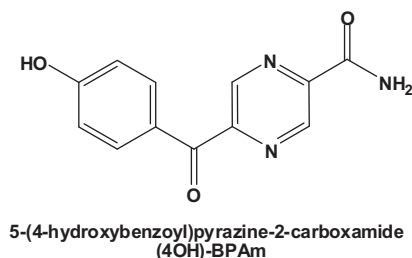
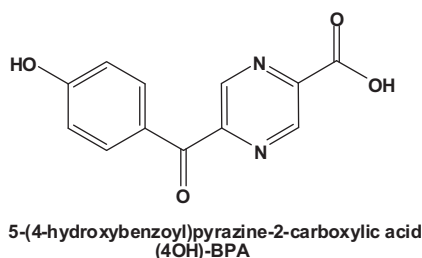
The azine ligands have energetically low lying π -antibonding orbitals, which can accept electrons from filled metal *d* orbitals. In consequence, they can exhibit charge transfer bands with interesting spectroscopic properties in the visible region [13]. Ligands containing pyrazine ring are widely studied and their π -donor properties are interesting. Its combination with other donor atoms should in principle afford complexes with tunable spectroscopic properties [14–16]. The hydride ligand – a powerful σ -donor – is found to be very efficient at compensating the electron deficiency at the metal central ion in complexes. The “trans effect” of H^- ligand and the interaction between carbonyl and donor ligands in *trans* positions to one another are stabilizing factors which explain stability of these complexes [17], are interesting due to their properties.

Here is reported an experimental and quantum chemical study of ruthenium hydride carbonyl complex with pyrazine derivative ligand. The quantum chemical study included a characterization of the molecular and electronic structures of the complex by analysis of optimized molecular geometry, electronic populations by using the natural bond orbitals scheme. The latter was used to identify the nature of the interactions between the ligands and the central ion. The calculated density of states showed the interactions and influences the orbital composition in the frontier electronic structure. The time dependent density functional theory

* Corresponding author.

E-mail address: gmalecki@us.edu.pl (J.G. Małecki).

(TD-DFT) was finally used to calculate the electronic absorption spectra. Based on a molecular orbital scheme, these results allowed the interpretation of the UV–Vis spectra obtained at an experimental level. The complex reported in this paper combine the interest in ruthenium hydride carbonyl coordination ligands and complexes containing nitrogen heterocyclic ligands [18–26].



2. Experimental

All free ligands were synthesized using modified method of Dolezal et al. [5]. Briefly, a stirred mixture of the 4-hydroxybenzaldehyde (120 mmol), and pyrazine-2-carboxamide or pyrazine-2-carboxylic acid (40 mmol) in 50% H₂SO₄ (80 ml) and 99% AcOH (80 ml) was cooled to –20 °C. To this mixture 80% *tert*-BuO₂H (13.5 g, 120 mmol) and a solution of FeSO₄·7H₂O (33.4 g, 120 mmol) in water were added simultaneously. The temperature must not exceed 0 °C. The resulting mixture was stirred for additional 3 h, during which the temperature was allowed to rise to room temperature. The reaction product (yellow crystals) was filtered and crystallized from MeOH.

The [RuHCl(CO)(PPh₃)₃] complex was synthesized according to the literature method [27].

2.1. Synthesis of 5-(4-hydroxybenzoyl)pyrazine-2-carboxylic acid

Yield = 14% IR: 3457, 3354 ν_{OH} ; 3057, 3000, 2947 ν_{PhH} ; 1914_{water}; 1698 ν_{COOH} ; 1640 ν_{CN} ; 1602 $\nu_{\text{C=C}}$; 1573 $\nu_{\text{as(COO)}}$; 1488 $\delta_{\text{(C-CH in the plane)}}$; 1451 ν_{Ph} ; 1357 $\nu_{\text{s(COO)}}$; 1297 $\nu_{\text{(C(O)-)}}$; 1273, 1165, 1038 $\delta_{\text{pyz ring}}$; 1013 $\delta_{\text{(CH in the plane)}}$; 940, 843 $\gamma_{\text{(pyz,Ph)}}$; 761 $\delta_{\text{(C(OH)=O)}}$; 621, 505 $\delta_{\text{(C-C out of the plane)}}$.

¹H-NMR (*d*₆-DMSO, 400 MHz): 10.66 (s, 1H, OH), 9.25 (m, 1H, pyrazine), 9.14 (m, 1H, pyrazine), 7.93 (d, 2H, *J* = 7.2 Hz, ArH), 6.91 (d, 2H, *J* = 7.6 Hz, ArH).

¹³C-NMR (*d*₆-DMSO, 100 MHz): 190.2, 165.1, 163.5, 152.9, 145.2, 144.9, 144.3, 134.0, 126.8, 115.9. UV–Vis (methanol, λ [nm]): 370.2 (1.20), 311.5 (2.21), 277.5 (3.20), 204.5 (4.38) MP: 195–196 °C.

2.2. Synthesis of the 5-(4-hydroxybenzoyl)pyrazine-2-carboxamide

Yield: 12% IR: 3438 $\nu_{\text{OH/NH}}$; 3192 ν_{PhH} ; 1922_{water}; 1687 $\nu_{\text{CO-NH}_2}$; 1634 ν_{CN} ; 1597 $\nu_{\text{C=C}}$; 1478 $\delta_{\text{(C-CH in the plane)}}$; 1448 ν_{Ph} ; 1415 ν_{CONH} ; 1384, 1298 $\nu_{\text{(C(O)-)}}$; 1278, 1168 $\delta_{\text{pyz ring}}$; 1034 $\delta_{\text{(CH in the plane)}}$; 927, 843 $\gamma_{\text{(pyz,Ph)}}$; 540, 508 $\delta_{\text{(C-C out of the plane)}}$.

¹H-NMR (*d*₆-DMSO, 400 MHz): 10.55 (s, 1H, OH), 9.23 (d, 1H, *J* = 1.3 Hz, pyrazine), 9.06 (d, 1H, *J* = 1.3 Hz, pyrazine), 8.43 (bs, 1H, NH₂), 7.99 bs 1H (NH₂), 7.96–7.88 (m, 2H, ArH), 6.94–6.87 (m, 2H, ArH). ¹³C-NMR: (*d*₆-DMSO, 100 MHz): 190.2, 164.9, 163.2, 152.6, 146.2, 143.8, 142.2, 134.0, 126.7, 115.6.

UV–Vis (methanol, λ [nm]): 360.2 (1.18), 312.2 (2.17), 273.8 (3.02), 214.6 (4.27). MP: 235 °C (lit [5], 235–236 °C).

2.3. Synthesis of the complexes

[RuHCl(CO)(PPh₃)₃] (0.2 mmol) and equimolar quantities of 5-(4-hydroxybenzoyl)pyrazine-2-carboxylic acid ((4-OH)BPA) and

5-(4-hydroxybenzoyl)pyrazine-2-carboxamide ((4-OH)BPAM) in CH₃OH (80 cm³) were refluxed until the complex suspension dissolved and also 1 h longer. The reaction solution was filtered and the single crystals were obtained by slow evaporation of solvent.

[RuH(CO)((4-OH)BPA)(PPh₃)₂].CH₃OH·H₂O (**1**): IR: 3565, 3495 ν_{OH} ; 3054 ν_{PhH} ; 2923 $\nu_{\text{CH(methanol)}}$; 1970; 1938 $\nu_{\text{RuCO/RuH}}$; 1626 $\nu_{\text{as(COO)}}$; 1603 $\nu_{\text{CN/C=C}}$; 1573 $\nu_{\text{as(COO)}}$; 1479 $\delta_{\text{(C-CH in the plane)}}$; 1434 $\nu_{\text{Ph(P-Ph)}}$; 1339 $\nu_{\text{s(COO)}}$; 1284, 1274, 1171, 1092 $\delta_{\text{(pyz ring)}}$; 1013 $\delta_{\text{(CH in the plane)}}$; 862 $\delta_{\text{(Ru-H)}}$; 744 $\delta_{\text{(C-C out of the plane)}}$; 517, 496 $\nu_{\text{(COO-Ru-P)}}$.

¹H NMR (400 MHz, CDCl₃) δ 8.39 (d, *J* = 2.9 Hz, pyz), 8.12–7.66 (m, PPh₃), 7.61 (d, *J* = 2.1 Hz, Ph), 7.25–7.21 (m, PPh₃), 7.01 (dd, *J* = 11.2, 6.7 Hz, Ph), 3.98 (s, OH), 3.51 (s, CH₃OH), 2.62–2.57 (m, H₂O), –9.57 (t, *J* = 19.3 Hz, Ru–H). ³¹P NMR (162 MHz, CDCl₃) δ : 43.83 (s, PPh₃). UV–Vis (methanol, λ [nm] (log ϵ)): 422 (1.16), 361 (1.39), 314 (2.37), 274 (4.76), 208 (4.28).

[RuH(CO)((4-OH)BPAM)(PPh₃)₂].2CH₃OH (**2**): IR: 3547, 3415 $\nu_{\text{OH/NH}}$; 3053 ν_{PhH} ; 2014; 1925 $\nu_{\text{RuCO/RuH}}$; 1652 ν_{CONH} ; 1598 $\nu_{\text{CN/C=C}}$; 1480 $\delta_{\text{(C-CH in the plane)}}$; 1433 $\nu_{\text{Ph(P-Ph)}}$; 1275, 1171, 1091 $\delta_{\text{(pyz ring/NH)}}$; 1027 $\delta_{\text{(CH in the plane)}}$; 844 $\delta_{\text{(Ru-H)}}$; 865 $\delta_{\text{(C-C out of the plane)}}$.

¹H NMR (400 MHz, CDCl₃) δ 9.77 (d, *J* = 101.9 Hz, pyz), 8.32, 8.18 (s, Ph), 7.88–7.24 (m, PPh₃), 6.96 (s, Ph), 6.08 (d, *J* = 150.0 Hz, NH), 3.51 (s, OH), –9.80 (t, *J* = 18.3 Hz, Ru–H).

³¹P NMR (162 MHz, CDCl₃) δ : 44.86 (s), 44.57 (s). UV–Vis (methanol, λ [nm] (log ϵ)): 457 (1.16), 374 (1.29), 311 (2.47), 276 (4.56), 214 (4.88).

2.4. Physical measurements

Infrared spectrum was recorded on a Perkin Elmer spectrophotometer in the spectral range 4000–450 cm^{–1} using KBr pellet. Electronic spectrum was measured on a Lab Alliance UV–Vis 8500 spectrophotometer in the range of 600–180 nm in methanol solution. ¹H ¹³C and ³¹P NMR spectra were obtained at room temperature in CDCl₃ or *d*₆-DMSO using a Bruker 400 spectrometer. Luminescence measurement was made in methanolic solution on an F-2500 FL spectrophotometer at room temperature.

2.5. Computational methods

The calculations were carried out using GAUSSIAN09 [28] program. Molecular geometry of the singlet ground state of the complex was

fully optimized in the gas phase at the B3LYP/DZVP level of theory [29,30]. For the compound a frequency calculation was carried out, verifying that the optimized molecular structure obtained corresponds to energy minimum, thus only positive frequencies were expected. The DZVP basis set [31] with f functions with exponents 1.94722036 and 0.748930908 was used to describe the ruthenium atom and the basis set used for the lighter atoms (C, N, O, P, H) was 6-31G with a set of “d” and “p” polarization functions. The TD-DFT (time dependent density functional theory) method [32] was employed to calculate the electronic absorption spectra of the complexes in the solvent PCM (Polarizable Continuum Model) model. In this work 90 singlet excited states were calculated as vertical transitions for the complexes. A natural bond orbital (NBO) analysis was also performed for all the complexes using the NBO 5.0 package [33] included in GAUSSIAN09. Natural bond orbitals are orbitals localized on one or two atomic centers, that describe molecular bonding in a manner similar to a Lewis electron pair structure, and they correspond to an orthonormal set of localized orbitals of maximum occupancy. NBO analysis provides the contribution of atomic orbitals (s, p, d) to the NBO σ and π hybrid orbitals for bonded atom pairs. In this scheme, three NBO hybrid orbitals were defined, bonding orbital (BD), lone pair (LP), and core (CR), which were analyzed on the atoms directly bonded to or presenting some kind of interaction with the ruthenium atom. The contribution of a group (ligands, central ion) to a molecular orbital was calculated using Mulliken population analysis. GAUSSSUM 2.2 [34] was used to calculate group contributions to the molecular orbitals and to prepare the partial density of states (DOS) spectra. The DOS spectra were created by convoluting the molecular orbital information with Gaussian curves of unit height and FWHM (Full Width at Half Maximum) of 0.3 eV.

2.6. Crystal structure determination and refinement

X-ray intensity data were collected with graphite monochromated Mo K α radiation at temperature of 295.0(2) K, with ω scan mode using the Oxford Diffraction Gemini A Ultra diffractometer.

Table 1

Crystal data and structure refinement details of (4-OH)BPA, [RuH(CO)((4-OH)BPA)(PPh₃)₂].CH₃OH·H₂O (1), (4-OH)BPAm and [RuH(CO)((4-OH)BPAm)(PPh₃)₂].2CH₃OH (2).

	C ₁₂ H ₈ N ₂ O ₄ ·2(H ₂ O)	C ₄₉ H ₃₈ N ₂ O ₅ P ₂ Ru·CH ₄ O·H ₂ O	C ₁₂ H ₉ N ₃ O ₃ ·H ₂ O	C ₄₉ H ₃₉ N ₃ O ₄ P ₂ Ru·2(CH ₄ O)
Empirical formula	C ₁₂ H ₈ N ₂ O ₄ ·2(H ₂ O)	C ₄₉ H ₃₈ N ₂ O ₅ P ₂ Ru·CH ₄ O·H ₂ O	C ₁₂ H ₉ N ₃ O ₃ ·H ₂ O	C ₄₉ H ₃₉ N ₃ O ₄ P ₂ Ru·2(CH ₄ O)
Formula weight	280.24	947.88	261.24	960.93
Temperature (K)	295.0(2)	295.0(2)	295.0(2)	960.93
Crystal system	triclinic	triclinic	triclinic	monoclinic
Space group	<i>P</i> $\bar{1}$	<i>P</i> $\bar{1}$	<i>P</i> $\bar{1}$	<i>P</i> 2 ₁ / <i>n</i>
Unit cell dimensions				
<i>a</i> (Å)	6.7346(5)	11.2730(5)	6.6417(4)	17.9948(16)
<i>b</i> (Å)	7.2143(5)	13.1500(6)	7.1466(5)	15.4596(8)
<i>c</i> (Å)	13.9007(10)	15.0795(7)	13.4848(9)	18.8528(16)
α (°)	86.321(6)	90.857(4)	85.194(6)	90
β (°)	82.561(6)	94.858(3)	76.503(5)	117.001(11)
γ (°)	66.713(7)	95.041(4)	67.397(6)	90
Volume (Å ³)	615.06(7)	2218.17(18)	574.57(7)	4673.0(8)
<i>Z</i>	2	2	2	4
<i>D</i> _{calc} (mg/m ³)	1.513	1.419	1.510	1.366
Absorption coefficient (mm ⁻¹)	0.123	0.481	0.116	0.456
<i>F</i> (000)	292	976	272	1984
Crystal dimensions (mm)	0.24 × 0.06 × 0.04	0.22 × 0.06 × 0.04	0.17 × 0.10 × 0.05	0.15 × 0.11 × 0.09
θ range for data collection (°)	3.39–25.05	3.37–25.05	3.41–25.05	3.38–25.05
Index ranges	–8 ≤ <i>h</i> ≤ 8 –8 ≤ <i>k</i> ≤ 8 –16 ≤ <i>l</i> ≤ 16	–13 ≤ <i>h</i> ≤ 13 –15 ≤ <i>k</i> ≤ 15 –17 ≤ <i>l</i> ≤ 17	–7 ≤ <i>h</i> ≤ 7 –8 ≤ <i>k</i> ≤ 8 –16 ≤ <i>l</i> ≤ 16	–20 ≤ <i>h</i> ≤ 21 –18 ≤ <i>k</i> ≤ 18 –22 ≤ <i>l</i> ≤ 19
Reflections collected	8729	20792	4747	25126
Independent reflections (<i>R</i> _{int})	2165 (0.0542)	7840 (0.0558)	2029 (0.0209)	2029 (0.0479)
Data/restraints/parameters	2165/0/189	7840/0/569	2029/0/216	8256/0/580
Goodness-of-fit on <i>F</i> ²	0.979	0.946	1.068	1.051
Final <i>R</i> indices [<i>I</i> > 2 σ (<i>I</i>)]	<i>R</i> ₁ = 0.0402 <i>wR</i> ₂ = 0.0844	<i>R</i> ₁ = 0.0444 <i>wR</i> ₂ = 0.0810	<i>R</i> ₁ = 0.0371 <i>wR</i> ₂ = 0.0882	<i>R</i> ₁ = 0.0602 <i>wR</i> ₂ = 0.1529
<i>R</i> indices (all data)	<i>R</i> ₁ = 0.0759 <i>wR</i> ₂ = 0.0910	<i>R</i> ₁ = 0.0763 <i>wR</i> ₂ = 0.0873	<i>R</i> ₁ = 0.0500 <i>wR</i> ₂ = 0.0938	<i>R</i> ₁ = 0.0922 <i>wR</i> ₂ = 0.1678
Largest diff. Peak and hole (eÅ ⁻³)	0.165 and –0.189	0.582 and –0.456	0.138 and –0.200	1.020 and –0.700

Lorentz, polarization and empirical absorption correction using spherical harmonics implemented in SCALE3 ABSPACK scaling algorithm [CrysAlis RED, Oxford Diffraction Ltd., Version 1.171.29.2] were applied. The structure was solved by the direct method and subsequently completed by the difference Fourier recycling. All the non-hydrogen atoms were refined anisotropically using full-matrix, least-squares technique. All the hydrogen atoms were found from difference Fourier synthesis after four cycles of anisotropic refinement, and refined as “riding” on the adjacent carbon atom with individual isotropic temperature factor equal 1.2 times the value of equivalent temperature factor of the parent atom. The OLEX2 [35] and SHELXS97, SHELXL97 [36] programs were used for all the calculations. Details concerning crystal data and refinement are gathered in Table 1.

3. Results and discussion

All free ligands were synthesized using modified method of Dolezal et al. [5]. Briefly, a stirred mixture of the 4-hydroxybenzaldehyde (120 mmol), and pyrazine-2-carboxamide or pyrazine-2-carboxylic acid (40 mmol) in 50% H₂SO₄ (80 ml) and 99% AcOH (80 ml) was cooled to –20 °C. To this mixture 80% *tert*-BuO₂H (13.5 g, 120 mmol) and a solution of FeSO₄·7H₂O (33.4 g, 120 mmol) in water were added simultaneously. The temperature must not exceed 0 °C. The resulting mixture was stirred for additional 3 h, during which the temperature was allowed to rise to room temperature. The reaction product (yellow crystals) was filtered and crystallized from MeOH. The complexes were synthesized by simply reactions between [RuHCl(CO)(PPh₃)₃] and equimolar quantities of the ligands in refluxed methanolic solutions.

3.1. Spectroscopic characterization of the ligands and complexes

The structures of the 5-(4-hydroxybenzoyl)pyrazine-2-carboxylic acid and amide derivative were confirmed by 2D-NMR techniques (COSY, HMQC and NOESY experiments). In addition the

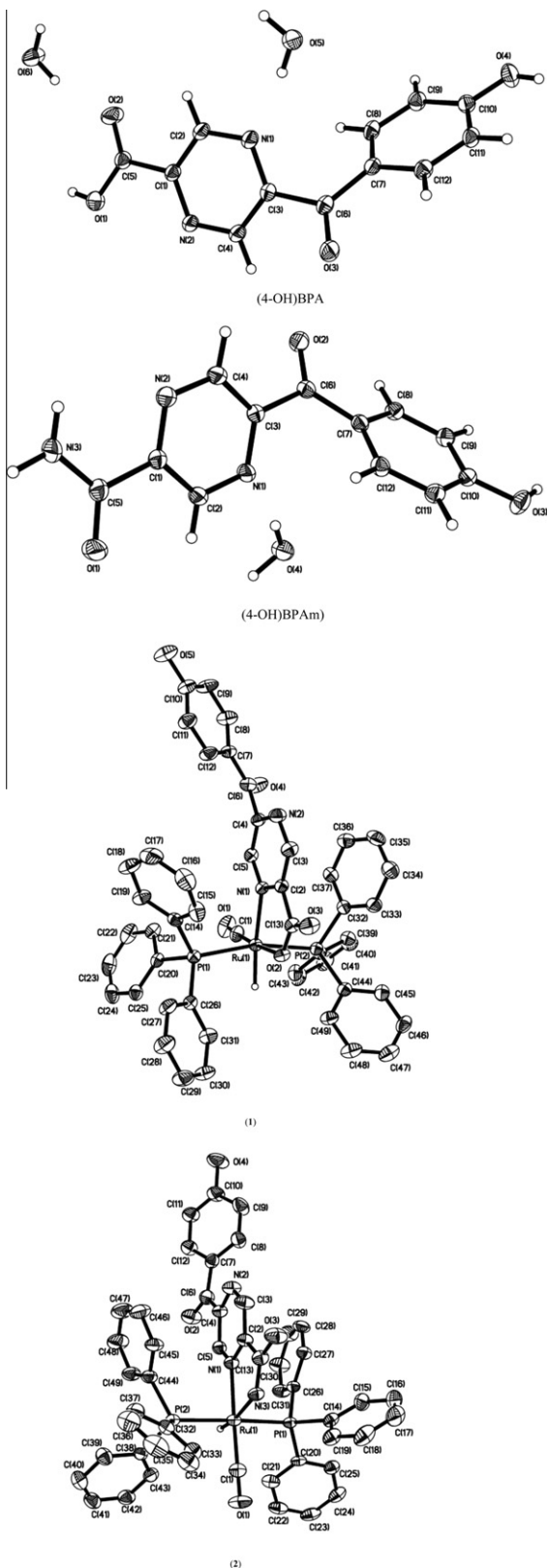


Fig. 1. ORTEP drawing of (4-OH)BPA, (4-OH)BPAm ligands and $[\text{RuH}(\text{CO})((4\text{-OH})\text{BPA})(\text{PPh}_3)_2]$, $[\text{RuH}(\text{CO})((4\text{-OH})\text{BPAm})(\text{PPh}_3)_2]$ complexes with 30% probability thermal ellipsoids. Hydrogen atoms except H(1Ru) and solvent molecules in the complexes structures are omitted for clarity.

values of proton conjugation constants in pyrazine ring ($J = 1.3 \text{ Hz}$) can be associated only with this regioisomers.

The ^{31}P NMR spectra of the complexes show singlet at 43.83 ppm in the case of complex (1) and two close together singlets at 44.86 and 44.57 ppm on the spectrum of complex (2). The ^1H NMR spectra of the complexes show set of signals corresponding to the PPh_3 ligands and the aromatic protons of the ligands. The OH and NH protons gave signals at 3.98, 3.51 and 6.08 ppm, respectively. The signals at high field (-9.57 and 9.80 ppm) indicate the presence of the hydride coordinated with the ruthenium. The shifts of the signals are due to the shielding effect of the metal and to the charge of the hydrogen atom. The signals are triplets due to coupling with the two *trans* equivalent phosphorus atoms ($J_{\text{HP}} \sim 19.3$ and 18.3 Hz). The complexes display strong Ru–H and C=O bands at 1970 , 1938 cm^{-1} and 2014 , 1925 cm^{-1} . The considerable difference in the Ru–H stretching band in the complexes suggests stronger interaction of hydride ligand with ruthenium(II) central ion in complex (2). The C=N and C=C stretching bands in the free ligands have maxima at 1640 , 1602 cm^{-1} and 1634 , 1597 cm^{-1} , respectively. In the complexes the C=N bands are shifted by about 36 cm^{-1} which supports efficient back donation from $d\pi_{\text{Ru}}$ to antibonding π^*_{pyz} orbitals. The stretching modes of carboxyl group in the complex (1) and amide in (2) are decreased by 78 and 36 cm^{-1} compared with free ligands which indicate the coordination of ruthenium central ions by the COO^- and $\text{C}(\text{O})\text{NH}_2$ groups, respectively.

3.2. Molecular structure

The ligands crystallise in $P\bar{1}$ space groups and the complexes in triclinic $P\bar{1}$ and monoclinic $P2_1/n$ space groups, respectively. Fig. 1 presents the molecular structures of the ligands and complexes and the selected bond distances and angles are collected in Table 2. The structures of the complexes can be considered as a distorted octahedral. The angles between ligands are different than expected for regular octahedron such as $82.5(9)^\circ$ for $\text{C}(1)\text{--Ru}(1)\text{--H}(1)$ and $79.8(9)^\circ$ for $\text{P}(2)\text{--Ru}(1)\text{--H}(1)$. The $\text{P}(1)\text{--Ru}(1)\text{--P}(2)$ angles are lower than 180° ($166.16(3)^\circ$ and $173.99(4)^\circ$). As one can see the angle between triphenylphosphine ligands in complex (1) more deviates from the ideal angle and on the ^{31}P NMR spectrum one signal is visible. In the structure of the complex electronic interaction ($\pi\text{--}\pi$ stacking) between PPh_3 phenyl and pyrazine ring exists with the plane-to-plane distance of 3.609 \AA . The interaction may explain the equivalence of the phosphorus in the solution of the complex. In the complex (2) there is no such interaction and two ^{31}P signals are presented on the NMR spectrum. In the molecular structure of the complexes the $\pi\text{--}\pi$ stacking interactions are visible. In the complex (2) the phenyl ring of PPh_3 ligand and the 4-hydroxyphenyl ring are T-shaped with distance 2.890 \AA as is presented on Fig. 2. In the crystal structures of the complexes intra- and inter-molecular hydrogen bonds exist [37] collected in Table 3.

The $\text{Ru}(1)\text{--C}(1)$ bond length in the complex (2) is longer by 0.03 \AA than in complex (1) and accordingly $\text{C}(1)\text{--O}(1)$ is shorter by 0.011 \AA in complex (2). In the structure of complex (1) the carbonyl ligand is in *trans* position to carboxyl group of the (4-HO)BPA ligand. The electron-donor COO^- group at $\text{Ru}(\text{II})$ ion delivers electron density via backbonding to the anti-bonding orbitals of the CO and produces a decrease in the carbonyl bond length. Additionally the decreasing of the CO vibration frequencies from 2014 to 1970 cm^{-1} in the complexes (1) and (2), respectively indicate the differences in the acceptor properties of carboxylic acid and amide ligands. In fact, by reducing the electron density on the metal the carbonyl ligand it will receive the electron density via $d\pi \rightarrow \pi^*$ interaction, which would increase the bond order, in turn increasing the vibration frequency of the CO bond. So it can be said that the amide ligand behave as weaker donor with respect to the carboxylic derivative. In the complexes considerable differences are in the Ru–H bond lengths. Knowing about the limits of Fourier

Table 2
Selected bond lengths [Å] and angles [°] for [RuH(CO)((4-OH)BPA)(PPh₃)₂]-CH₃OH·H₂O (**1**) and [RuH(CO)((4-OH)BPAm)(PPh₃)₂]-2CH₃OH (**2**) with the optimized geometry values.

	(1)		(2)	
	Exp.	Calc.	Exp.	Calc.
<i>Bond lengths (Å)</i>				
Ru(1)–C(1)	1.812(4)	1.857	1.842(5)	1.864
Ru(1)–N(1)	2.162(2)	2.232	2.147(4)	2.190
Ru(1)–O(2)/N(3)	2.149(2)	2.161	2.168(4)	2.207
Ru(1)–H(1)	1.61(3)	1.62	1.26(4)	1.64
Ru(1)–P(1)	2.3741(9)	2.435	2.341(13)	2.427
Ru(1)–P(2)	2.3489(9)	2.433	2.351(13)	2.427
C(1)–O(1)	1.163(4)	1.164	1.152(6)	1.165
C(13)–O(2)				
[free ligand]	1.271(4)			
[1.205(2)]	1.229			
C(13)–O(3)				
[free ligand]	1.229(4) [1.302(2)]	1.297	1.262(6) [1.2282(18)]	1.244
C(13)–N(3)				
[free ligand]			1.288(6) [1.319(2)]	1.335
<i>Angles (°)</i>				
O(2)/N(3)–Ru(1)–C(1)	175.83(13)	174.86	103.3(2)	105.79
N(1)–Ru(1)–C(1)	101.03(13)	99.68	177.5(2)	179.68
N(3)/O(2)–Ru(1)–N(1)	75.69(9)	75.19	74.37(15)	74.53
C(1)–Ru(1)–P(2)	92.06(11)	89.92	90.10(17)	88.88
O(2)/N(3)–Ru(1)–P(2)	85.77(6)	90.97	91.60(11)	91.63
N(1)–Ru(1)–P(2)	95.82(7)	95.95	90.88(11)	91.09
C(1)–Ru(1)–P(1)	94.16(11)	95.02	89.02(17)	88.82
O(2)/N(3)–Ru(1)–P(1)	88.73(6)	85.33	94.39(11)	91.86
P(1)–Ru(1)–N(1)	95.11(7)	96.56	90.24(11)	91.19
P(2)–Ru(1)–P(1)	166.16(3)	165.58	173.99(4)	176.24
C(1)–Ru(1)–H(1)	82.5(9)	89.00	87(2)	89.00
O(2)/N(3)–Ru(1)–H(1)	100.6(9)	96.00	169(2)	166.00
N(1)–Ru(1)–H(1)	174.6(9)	172.00	95(2)	91.00
P(2)–Ru(1)–H(1)	79.8(9)	83.00	87.0(19)	89.00
P(1)–Ru(1)–H(1)	88.7(9)	84.00	87.0(19)	88.00
Ru(1)–C(1)–O(1)	178.1(3)	175.70	179.0(5)	179.56

synthesis and the problems in recognizing artifacts in the immediate neighborhood of heavy atoms it is doubtful if a reliable position for the hydrogen atom bound to the Ru-atom can be found in the difference Fourier map avoiding the danger of mistaking the effects of the series termination errors for a true atomic position. In the studied complexes that is very possible taking into account the bond lengths in complex (**2**) of 1.26(4) Å shorter than in (**1**) about 0.35 Å but the ruthenium-hydride distances are known [38,39]. In the complex (**2**) the hydride ligand is in *trans* position to amide nitrogen donor. As one can see from the data in Table 2 the C–N_{amide} bond length in the free ligand is reduced in complex by about 0.031 Å and the amide C=O bond increases to 1.262(6) Å. The electron-donor hydride ligand at Ru(II) ion delivers electron density via backbonding to the anti-bonding orbitals of the amide and produces a significant decrease of about 35 cm⁻¹ in the vibration frequency of the coordinated amide compared to free ligand. The electronic effects are supported by theoretically determined charge values which indicate the more negative charge of Ru(II) central ion (–0.83) in (**2**) than in complex (**1**) (–0.72). Additionally the charges on the hydride ions are also different in the complexes 0.05 in (**1**) and 0.01 in complex (**2**).

3.3. Optimized geometries, hybrid and molecular orbitals description

The ground state geometries of the complexes were optimized in singlet states using the DFT method with the B3LYP functional. The calculations were carried out for gas phase molecules and in general, the predicted bond lengths and angles are in an agreement with the values based on the X-ray crystal structure data, and the general trends observed in the experimental data are reproduced in the calculations. The calculated IR frequencies of the complexes shown in Fig. 3 confirm calculated structures with experimental

ones and the differences in calculated and experimental spectra mainly result from the negligence of intermolecular interactions for the gas phase. From the data collected in Table 2, one may see that the majority of differences between the experimental and calculated geometries are found in the Ru–P distance (~0.08 Å) and the maximum angle differences are visible in C(1)–Ru(1)–H(1) 6.5°. The C≡O bond length does not undergo important change and slight increase of ~0.013 Å is seen.

The NBO analyses were performed for the complexes which allowed knowing the nature of the coordination between ruthenium and the atoms of the ligands directly interacting with it. This methodology also gave a better understanding of the optimized molecular structures. In the analysis was found that the N,O- and N,N-donor ligand does not show covalent bonding with ruthenium. The Coulomb-type interaction between the ruthenium central ions and pyrazine carboxylic acid and amide derivative ligands is clearly visible in the calculated Wiberg bond indices whose values are considerably lower than one. The Ru–N_{pyz} and Ru–O bond indices for complex (**1**) are close to 0.38 and 0.41 and in the complex (**2**) the ruthenium pyrazine nitrogen bond is slightly more covalent (*W* = 0.48) and the Wiberg index for Ru–N_{amide} is 0.42. The Ru–P bond orders are also smaller than 1 (~0.7). For the carbonyl group of the complex, three natural bond orbitals were detected for the C≡O bond, and one for the Ru–C bond. The Ru–C bond orbitals are polarized towards the carbon atom, and the C=O bond orbitals are polarized towards the oxygen end. The oxygen atom of the carbonyl ligand has one lone pair (LP) orbital. The charges of CO ligands can be easily calculated by summing the individual charges on the carbon and oxygen atoms and have values 0.19 in both complexes. The Wiberg indexes of the CO bonds in the complexes are reduced by about 0.23 with respect to free CO (*W*_{CO} = 2.23) and the *W*_{Ru–C} in the complexes have values 1.34

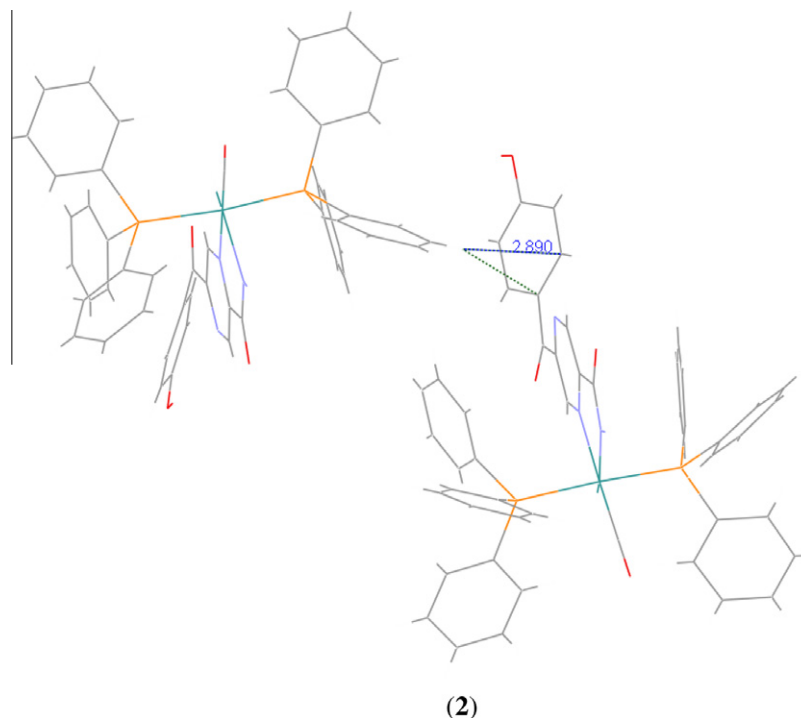


Fig. 2. The p-stacking interactions in the $[\text{RuH}(\text{CO})((4\text{-OH})\text{BPAm})(\text{PPh}_3)_2]$ (**2**) complex. The distances are in [Å]. The position of the molecule #2 is generated by $1 - x$, $1 - y$, $-z$ symmetry operation.

Table 3

Hydrogen bonds for $[\text{RuH}(\text{CO})((4\text{-OH})\text{BPAm})(\text{PPh}_3)_2] \cdot \text{CH}_3\text{OH} \cdot \text{H}_2\text{O}$ (**1**) and $[\text{RuH}(\text{CO})((4\text{-OH})\text{BPAm})(\text{PPh}_3)_2] \cdot 2\text{CH}_3\text{OH}$ (**2**) (Å and °).

D–H...A	d(D–H)	d(H...A)	d(D...A)	∠(DHA)
(1)				
O(5)–H(5A)...O(6) #1	0.82	1.79	2.581(4)	161.1
O(6)–H(6)...O(3) #2	0.73	2.06	2.776(4)	167.0
O(7)–H(7A)...O(4) #3	0.85	2.11	2.953(4)	172.4
O(7)–H(7B)...O(3) #4	0.85	1.99	2.820(4)	166.7
C(45)–H(45)...O(7)	0.93	2.57	3.358(6)	142.5
C(49)–H(49)...O(2)	0.93	2.51	3.067(4)	118.8
(2)				
O(4)–H(4)...O(6)	0.82	1.85	2.640(7)	159.8
O(5)–H(5A)...O(3)	0.82	1.82	2.635(6)	176.6
O(6)–H(6)...O(5) #5	0.82	1.88	2.696(8)	170.9
C(8)–H(8)...N(2)	0.93	2.36	2.861(7)	113.5
C(42)–H(42)...O(3) #6	0.93	2.58	3.383(8)	144.9

Symmetry transformations used to generate equivalent atoms: #1 $1 - x$, $1 - y$, $-z$; #2 $1 + x$, y , z ; #3 $1 - x$, $1 - y$, $1 - z$; #4 $-x$, $1 - y$, $1 - z$; #5 x , $-1 + y$, z ; #6 $1/2 + x$, $3/2 - y$, $1/2 + z$.

and 1.32 in complexes (**1**) and (**2**), respectively. These weak values are in agreement with the elongation of the $\text{C}\equiv\text{O}$ bond in complexes and charge distribution in the terminal bonding carbonyl group to ruthenium central ion. Moreover these points to rather small differences in the properties of donor–acceptor of studied pyrazine derivatives manifested as evidenced by the acceptance of charge by a carbonyl ligand in the complexes. Additionally similar values are in the ruthenium(II) complexes with pyrazine (1.31) [26], pyrazine-2-carboxylic acid and pyrazine-2,3-dicarboxylic acid ligands ($W_{\text{Ru-C}} = 1.35$) [40]. The similar values of Wiberg indexes suggest almost the same donor–acceptor properties of the pyrazine and its derivatives. The natural charges on the ruthenium central ions are -0.72 for (**1**) and -0.83 for (**2**) and the occupancies of the ruthenium d orbitals are as follows: (**1**) $d_{xy} - 1.84$; $d_{xz} - 1.70$; $d_{yz} - 1.73$; $d_{x^2-y^2} - 1.31$; $d_{z^2} - 1.01$ and (**2**) $d_{xy} - 1.68$; $d_{xz} - 1.66$;

$d_{yz} - 1.90$; $d_{x^2-y^2} - 1.16$; $d_{z^2} - 1.21$. The d -electron populations of 7.59 for (**1**) and 7.62 for (**2**) correspond to the oxidation state Ru(0), not to their formal oxidation state Ru(II). This is a supporting argument for ligands to d_{Ru} electron transfer. The data suggest that the donation from ligands to d_{Ru} orbitals plays a role in the electronic structure of the complexes, and in order to determine the donation, the stabilization energies¹ were calculated. The stabilization energies calculated in NBO analyses have shown that the lone pairs localized on the N(O/N)-donor atoms of ligands in the complexes donate the charge to ruthenium, and the stabilization energies (ΔE_{ij}) are 131.97 and 112.23 kcal/mol for (**1**) and (**2**), respectively. The back donations to pyrazine type ligands are equal to 33.34 and 43.21 kcal/mol for complexes (**1**) and (**2**), respectively and the data point out the higher π -acceptor properties of amide derivative.

Analysis of the frontier molecular orbitals is useful for understanding the spectroscopic properties as electronic absorption and emission spectra of organometallic complexes. The densities of states (DOS) in terms of Mulliken population analysis were calculated using the GAUSSSUM program and Fig. 4 presents the composition of the fragment orbitals contributing to the molecular orbitals for the studied complex and the insets present the overlap partial density of states. As one can see the π -acceptor interaction between carbonyl groups towards ruthenium(II) in complex (**1**) is smaller compared with interaction in complex (**2**). To compare the properties of the pyrazine and its derivatives as ligands on the Fig. 5 are presented the OPDOS diagrams for ruthenium hydride-carbonyl complexes with the ligands. As one can see the interaction of accepting properties of pyrazine is smaller than its carboxylic derivative (pyz-2-COO^-) and the amide ligand (4-HO)BPAm is strongest π -acceptor from these ligands.

¹ ΔE_{ij} (kcal/mol) associated with delocalization is estimated by the second-order perturbative as: $\Delta E_{ij} = q_i (F(i,j)^2) / (e_j - e_i)$ where q_i is the donor orbital occupancy, e_i , e_j are diagonal elements (orbital energies) and $F(i,j)$ is the off-diagonal NBO Fock or Kohn–Sham matrix element.

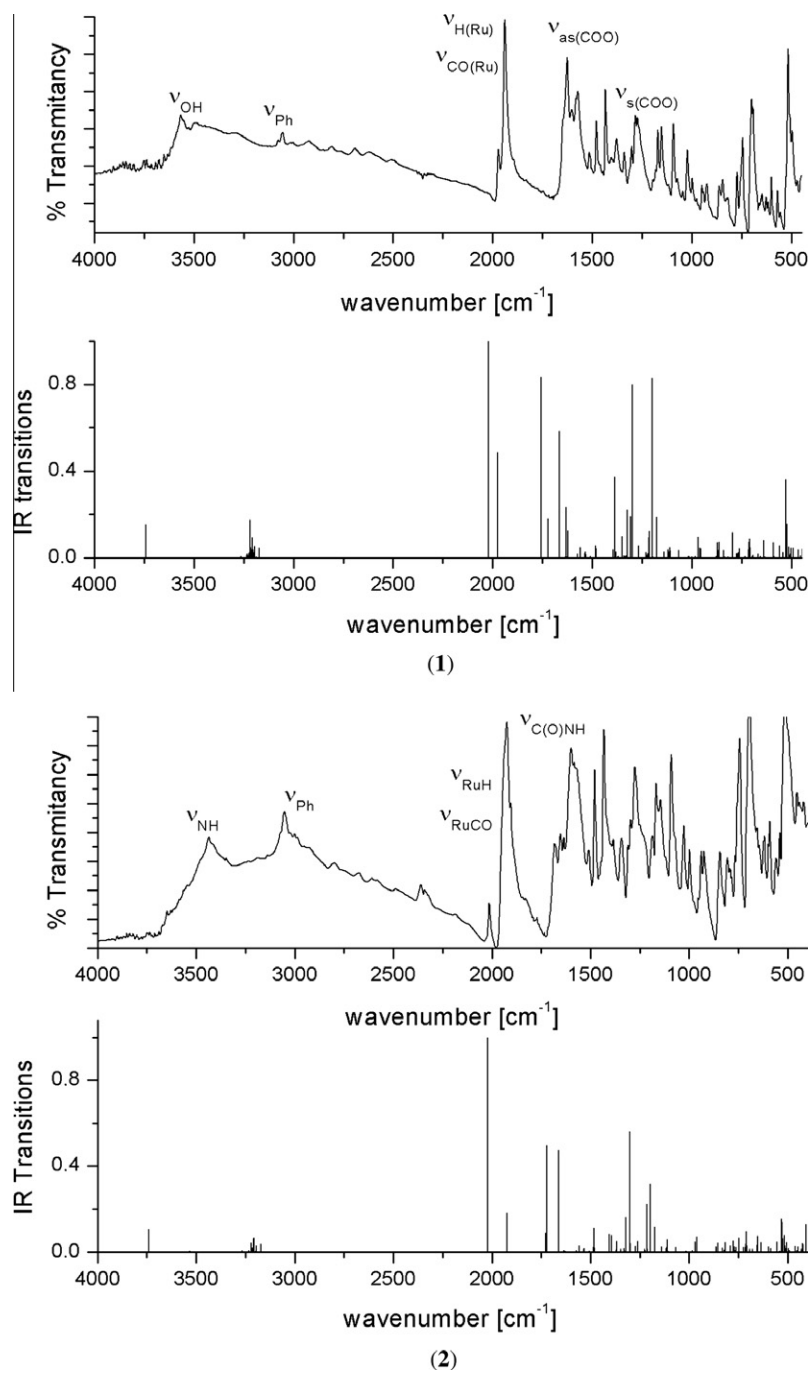


Fig. 3. Experimental and calculated IR spectra of $[\text{RuH}(\text{CO})((4\text{-OH})\text{BPA})(\text{PPh}_3)_2]$ and $[\text{RuH}(\text{CO})((4\text{-OH})\text{BPAm})(\text{PPh}_3)_2]$ complexes.

The electronic structures of the complexes are similar. The HOMOs are localized on the d ruthenium orbital (53% in (1) and 33% in (2)) with contribution of pyrazine derivative ligands. In the complexes d_{Ru} play significant role in HOMO–1 and HOMO–2 in the complex (1) and in the case of complex (2) in the HOMO–2 to HOMO–6 range. LUMO and LUMO+1 are localized on the pyrazine derivative ligands (97%) in both complexes as can be seen on the DOS diagrams in Fig. 4. The d_{z^2} and $d_{x^2-y^2}$ orbitals of ruthenium are visible in LUMO+2 orbitals (17% and 18%) and in higher virtual orbitals in the range of LUMO+16 to LUMO+19 with the contribution of π^* orbitals of carbonyl ligands. The difference in electronic structures of the complexes manifest itself in the HOMO–LUMO gaps 3.27 eV in (1) and 2.67 eV in complex (2). In the case of

complex (2) with amide derivative ligand the HOMO and HOMO–1 orbitals are shifted to higher energy and the ligand play dominant role in the frontier occupied orbitals.

3.4. Experimental and theoretical electronic spectra

The UV–Vis spectra of the complexes are similar and in the spectra the maxima close to 422, 361, 314 and 457, 374, 311 were measured. Based on the pseudo-octahedral geometry of the complex and taking into account the $d-d$ transitions assigned to $^1A_1 \rightarrow ^1T_1$ and $^1A_1 \rightarrow ^1T_2$ in octahedron (or $^1A_1 \rightarrow ^1A_2/B_1/E$ in lower symmetry fields), the ligand field parameters $10Dq$ can be estimated to 23468 cm^{-1} and 21514 cm^{-1} for complexes (1) and (2),

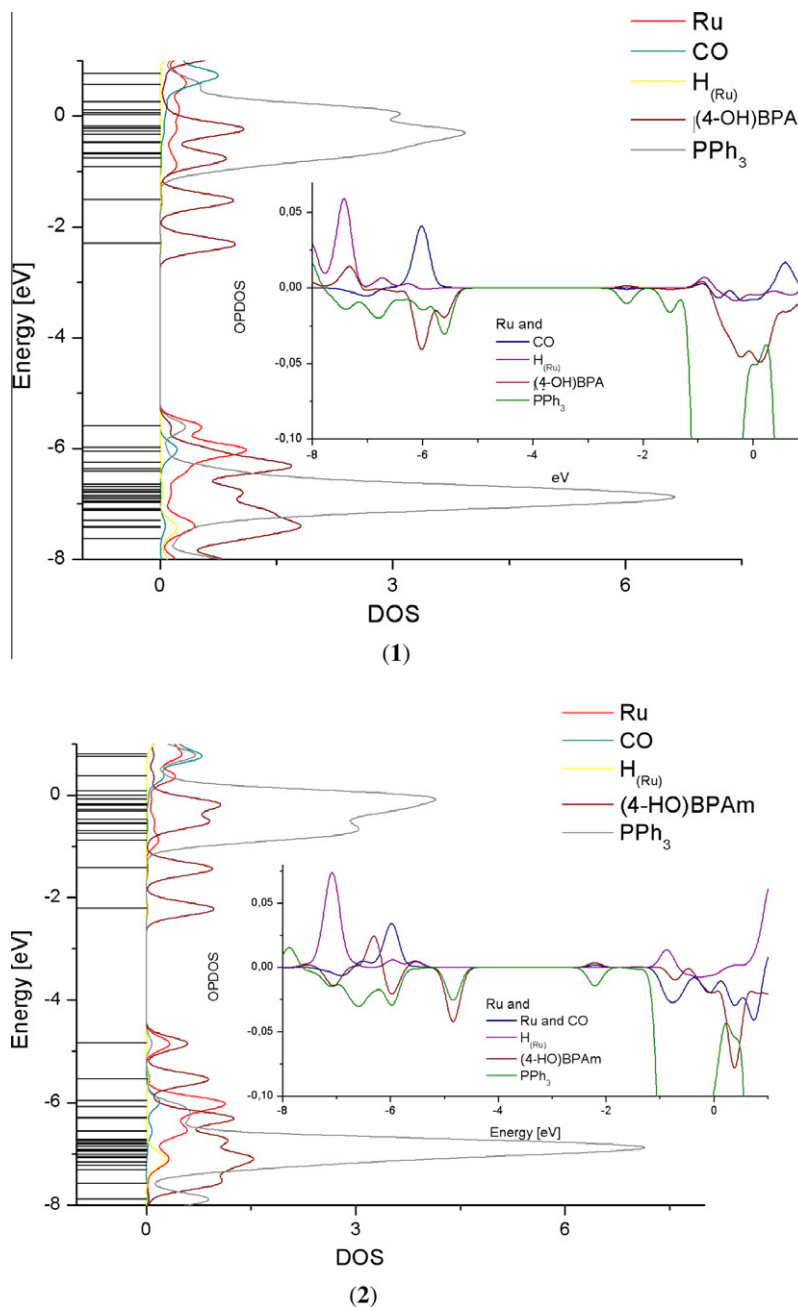


Fig. 4. The density-of-states diagrams with overlap density-of-states as inset diagram for $[\text{RuH}(\text{CO})((4\text{-OH})\text{BPA})(\text{PPh}_3)_2]$ and $[\text{RuH}(\text{CO})((4\text{-HO})\text{BPAm})(\text{PPh}_3)_2]$ complexes.

respectively. Adequately Racah's parameters are $B = 250$ and 304 cm^{-1} and the nephelauxetic parameters have values $\beta_{55} = 0.35$ and 0.42 . The bands observed in the vicinity of 300 nm have been attributed to intra- and interligand ($\pi_{\text{C}_6\text{H}_6}^b \rightarrow 3d_{\text{phosphorus}}$ and $\pi \rightarrow \pi_{\text{C}=\text{C}}$) transitions with admixture of *Metal-Ligand Charge Transfer* transitions ($d_{\text{Ru}} \rightarrow \pi_{\text{N,O/N-ligand}}^*$ and $d_{\text{Ru}} \rightarrow \pi_{\text{Ph}}^*$). The highest experimental band close to $208, 214 \text{ nm}$ may result from transitions in the PPh_3 ligands and from $\pi \rightarrow \pi^*$ excitations in the $\text{N,O/N-heteroaromatic}$ ligands.

In Table 4, several calculated electronic transitions and their assignments to the experimental absorption bands are gathered. The assignment of the calculated orbital excitations to the experimental bands was based on an overview of the composition and relative energy to the orbitals HOMO and LUMO involved in the electronic transitions. As can be seen most of the excitations have *Metal-to-Ligand Charge Transfer* character. The $d \rightarrow d$ transition was

calculated at 337.8 nm and 372.9 nm ($\text{HOMO} \rightarrow \text{L}+2$) in complexes (1) and (2), respectively but this is no "clear" *LF* transition due to contribution of ligands in HOMO and LUMO+2 molecular orbitals. The intraligand transitions ($\pi(\text{PPh}_3) \rightarrow \pi^*(\text{L})$) were calculated in the vicinity of 300 nm . The highest experimental band close to 210 nm may result from transitions in the PPh_3 and from $\pi \rightarrow \pi^*$ excitations in the pyrazine derivative ligands.

The emission characteristic of the complex (1) has been examined in the methanol solution (with concentration of $5 \times 10^{-4} \text{ mol/dm}^3$) at room temperature. The excitation at 301 nm gave fluorescence with maximum at 399 nm as presents Fig. 6a. The red shifts of the emission maximum is typical to ruthenium(II) complexes and the emission originating from the metal to ligand charge transfer (MLCT) state, derived from the excitation involving a $d_{\text{Ru}} \rightarrow \pi_{\text{ligand}}^*$ transition. The assignment is supported by the analysis of the frontier orbitals of the corresponding

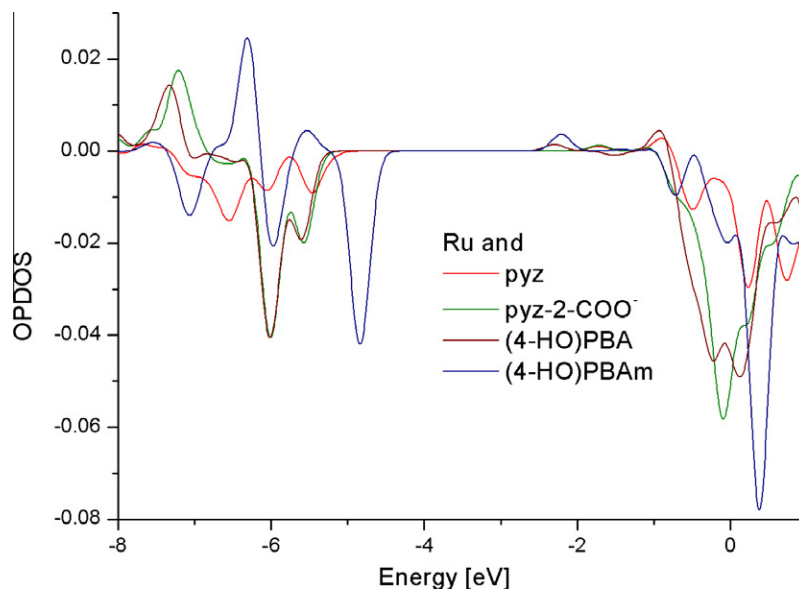


Fig. 5. The overlap partial density of states diagrams for interaction of ruthenium(II) central ions with pyrazine, pyrazine-2-carboxylic acid, (4-OH)BPA and (4-OH)BPAm ligands.

Table 4

The calculated electronic transitions and their assignments to the experimental absorption bands.

The most important orbital excitations	Character	λ (nm)	f	Experimental λ (nm)
(1)				
HOMO \rightarrow LUMO (98%)	$d \rightarrow \pi^*(L)$	460.5	0.0519	422
H-1 \rightarrow LUMO (88%)	$d \rightarrow \pi^*(L)$	413.9	0.0001	
H-3 \rightarrow LUMO (60%); H-2 \rightarrow LUMO (10%); HOMO \rightarrow L + 1 (18%)	$d \rightarrow \pi^*(L)$; $\pi(L) \rightarrow \pi^*(L)$	362.6	0.2528	361
HOMO \rightarrow L + 2 (61%); HOMO \rightarrow L + 3 (15%)	$d \rightarrow d/\pi^*(L)$	337.8	0.1262	
H-10 \rightarrow LUMO (19%); H-8 \rightarrow LUMO (36%); H-6 \rightarrow LUMO (14%); H-5 \rightarrow LUMO (14%)	$\pi(PPh_3) \rightarrow \pi^*(L)$; $\pi(L) \rightarrow \pi^*(L)$	320.9	0.0073	
H-2 \rightarrow LUMO (75%)	$d \rightarrow \pi^*(L)$	315.9	0.0032	314
H-7 \rightarrow L + 1 (10%); H-1 \rightarrow L + 2 (20%)	$\pi(PPh_3) \rightarrow \pi^*(L)$; $d \rightarrow d$	304.6	0.0278	
H-2 \rightarrow L + 2 (16%); HOMO \rightarrow L + 4 (20%); HOMO \rightarrow L + 10 (10%)	$d \rightarrow d$; $d \rightarrow \pi^*(PPh_3)$; $d \rightarrow \pi^*(L)$	299.8	0.0362	
H-18 \rightarrow LUMO (25%); H-7 \rightarrow L + 1 (29%)	$\pi(L/PPh_3) \rightarrow \pi^*(L)$	289.1	0.0317	
HOMO \rightarrow L + 6 (87%)	$d \rightarrow \pi^*(PPh_3)$	270.9	0.0282	274
H-20 \rightarrow LUMO (21%); H-19 \rightarrow LUMO (10%); H-2 \rightarrow L + 4 (10%)	$d \rightarrow \pi^*(L/PPh_3)$	268.6	0.051	
HOMO \rightarrow L + 7 (44%); HOMO \rightarrow L + 10 (15%)	$d \rightarrow \pi^*(L/PPh_3)$	264.1	0.0289	
H-4 \rightarrow L + 2 (49%)	$\pi(L) \rightarrow d$	260.6	0.3641	
(2)				
HOMO \rightarrow LUMO (97%)	$d \rightarrow \pi^*(L)$	564.1	0.0265	
HOMO \rightarrow L + 1 (97%)	$d \rightarrow \pi^*(L)$	426.5	0.0005	457
H-2 \rightarrow LUMO (94%)	$d \rightarrow \pi^*(L)$	396.0	0.0171	
HOMO \rightarrow L + 2 (80%)	$d \rightarrow d/\pi^*(PPh_3)$	372.9	0.0247	374
H-2 \rightarrow L + 1 (81%)	$d \rightarrow \pi^*(L)$	318.4	0.0339	
H-17 \rightarrow LUMO (67%)	$\pi(L) \rightarrow \pi^*(L)$	314.0	0.0038	311
HOMO \rightarrow L + 5 (61%)	$d \rightarrow \pi^*(PPh_3)$	306.95	0.019	
H-4 \rightarrow L + 1 (77%)	$d/\pi(PPh_3) \rightarrow \pi^*(L)$	296.3	0.1597	
H-5 \rightarrow L + 2 (16%); H-2 \rightarrow L + 2 (53%)	$d/\pi(PPh_3) \rightarrow d/\pi^*(PPh_3)$	290.8	0.1867	
HOMO \rightarrow L + 12 (58%)	$d \rightarrow \pi^*(PPh_3)$	276.9	0.0017	276
H-21 \rightarrow LUMO (32%); HOMO \rightarrow L + 14 (33%)	$\pi(L) \rightarrow \pi^*(L)$; $d \rightarrow \pi^*(PPh_3)$	267.1	0.1333	

L denotes (4-OH)BPA in (1) and (4-OH)BPAm in (2).

complex showing a contribution of ligands nature. Moreover in these regions were calculated the transitions composite from *Ligand-to-Ligand* and *Metal-to-Ligand Charge Transfer* ($\pi_{PPh_3} \rightarrow \pi^*_L$ and $d \rightarrow \pi^*_L$; $d \rightarrow \pi^*(PPh_3)$). The emission properties of 5-(4-hydroxybenzoyl)pyrazine-2-carboxylic acid is presented on the Fig. 6b. The methanolic solution of the ligand excited at 282 nm presents fluorescence with maximum at 330 nm.

The methanol solution of complex (2) was excited in the range between 270 and 600 nm and the emission was not observed. This lack of fluorescence is probably associated with the differences in

the electronic structure of the complexes and much larger participations of ligand in molecular orbitals taking part in MLCT transitions.

4. Conclusion

Two new benzoylpyrazine carboxylic acid ligands and its hydride-carbonyl complexes of ruthenium were synthesized and characterized by infra red, proton and phosphorus nuclear magnetic resonance, electronic absorption and emission spectroscopy and X-ray crystallography. In the crystal structure of the complexes

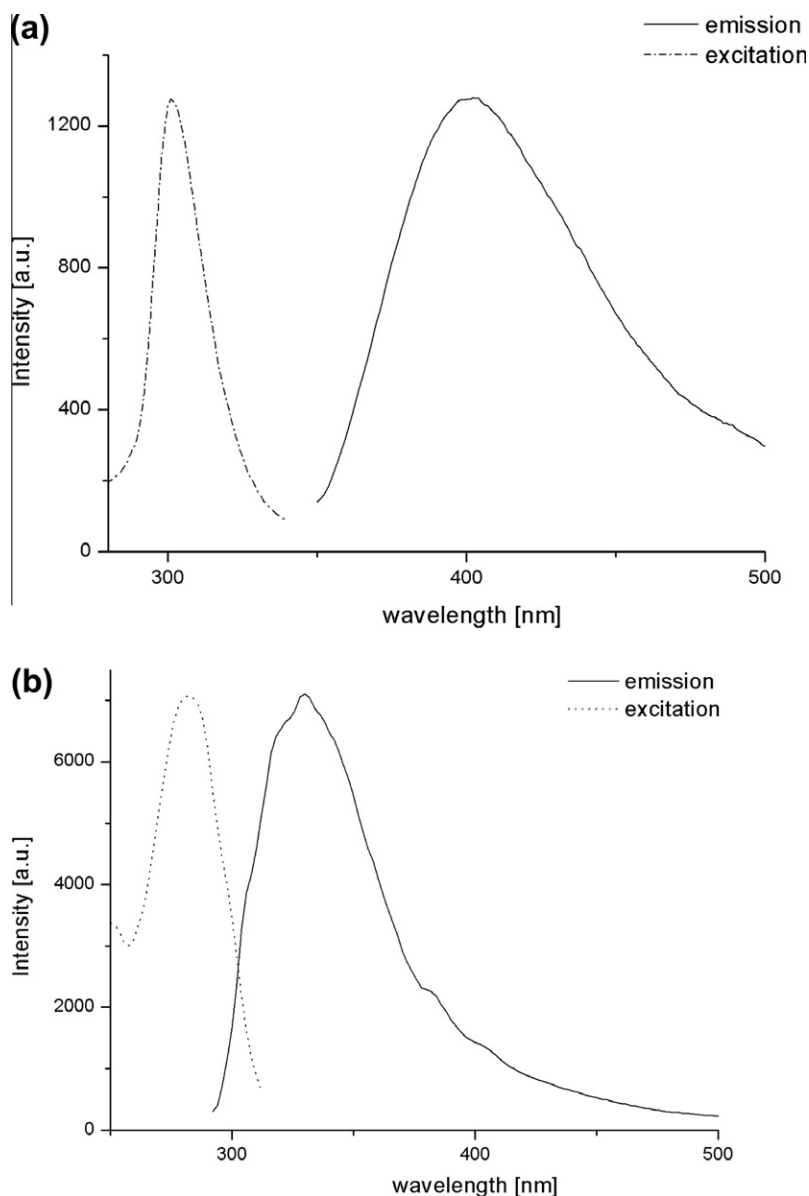


Fig. 6. Fluorescence spectra of $[\text{RuH}(\text{CO})((4\text{-OH})\text{BPA})(\text{PPh}_3)_2]\cdot\text{CH}_3\text{OH}\cdot\text{H}_2\text{O}$ (**1**) complex (a) and 5-(4-hydroxybenzoyl)pyrazine-2-carboxylic acid (**2**) in methanolic solutions.

two types of non-covalent interactions between aromatic rings (parallel-displaced and T-shaped) have been found.

Electronic structures of the complexes have been determined using the density functional theory (DFT) method, and employed for discussion of its properties. The NBO analyses point out the higher π -acceptor properties of amide derivative than carboxylic acid (4-OH)BPA ligand. The differences in the donor–acceptor properties of the amide and carboxylic ligands manifest itself in the considerable difference in the Ru–H stretching band in the complexes. The stronger COO donor is in *trans* to carbonyl ligand in complex (**1**) and the weaker amide donor in complex (**2**) occupies *trans* position to hydride. The electronic structures of these complexes, presented in particular by the density of states diagrams, have been correlated with their ability to fluoresce and used to analyze the UV–Vis spectra. The lack of luminescence in the case of complex (**2**) is probably associated with the smaller participation of ruthenium in molecular orbitals involved in MLCT transitions. The differences in frontier occupied molecular orbitals are clearly visible on the DOS diagrams. The amide derivative unlike carboxylic ligand causes the increase in the energy the HOMO's

and consequently dividing levels of d_{xy} , d_{xz} and d_{yz} ruthenium orbitals through ligand orbitals (HOMO–1 in complex (**2**) is localized (89%) on the (4-OH)BPAm ligand).

Acknowledgements

M. Serda was supported by a TWING fellowship and NCN grant DEC-2011/01/N/NZ4/01166. The GAUSSIAN-09 calculations were carried out in the Wrocław Centre for Networking and Supercomputing, WCSS, Wrocław, Poland, <http://www.wcss.wroc.pl>, under calculational Grant No. 18.

Appendix A. Supplementary data

CCDC 856480, 855434, 857547 and 864845 contain the supplementary crystallographic data for $\text{C}_{12}\text{H}_8\text{N}_2\text{O}_4\cdot 2(\text{H}_2\text{O})$, $\text{C}_{49}\text{H}_{38}\text{N}_2\text{O}_5\cdot \text{P}_2\text{Ru}\cdot\text{CH}_4\text{O}\cdot\text{H}_2\text{O}$, $\text{C}_{12}\text{H}_9\text{N}_3\text{O}_3\cdot\text{H}_2\text{O}$ and $\text{C}_{49}\text{H}_{39}\text{N}_3\text{O}_4\text{P}_2\text{Ru}\cdot 2(\text{CH}_4\text{O})$ compounds, respectively. These data can be obtained free of charge from <http://www.ccdc.cam.ac.uk/conts/retrieving.html>, or from the

Cambridge Crystallographic Data Centre, 12 Union Road, Cambridge CB2 1EZ, UK; fax: +44 1223 336 033; or e-mail: deposit@ccdc.cam.ac.uk.

References

- [1] C.H. Londergan, J.C. Salsman, S. Ronco, C.P. Kubiak, *Inorg. Chem.* 42 (2003) 926.
- [2] M.G. Sauaia, R.G. de Lima, A.C. Tedesco, R.S. da Silva, *JACS* 125 (2003) 14718.
- [3] V. Opletalova, D.S. Kalinowski, M. Vejsova, J. Kunes, M. Pour, J. Jampilek, V. Buchta, D.R. Richardson, *Chem. Res. Toxicol.* 21 (2008) 1878.
- [4] R. Rajagopalan, W.L. Neumann, A.R. Poreddy, R.M. Fitch, J.N. Freskos, B. Asmelash, K.R. Gaston, K.P. Galen, J. Shieh, R.B. Dorshow, *J. Med. Chem.* 54 (2011) 5048.
- [5] M. Dolezal, J. Jampilek, Z. Osicka, J. Kunes, V. Buchta, P. Vichova, *Farmaco* 58 (2003) 1105.
- [6] M. Dolezal, P. Cmedlova, L. Palek, J. Vinsova, J. Kunes, V. Buchta, J. Jampilek, K. Kralova, *Eur. J. Med. Chem.* 43 (2008) 1105.
- [7] L. Salvi, A. Salvini, F. Micoli, C. Bianchini, W. Oberhauser, *J. Organomet. Chem.* 692 (2007) 1442.
- [8] C. Po Lau, S. Man Ng, G. Jia, Z. Lin, *Coord. Chem. Rev.* 251 (2007) 2223.
- [9] C. Jun Yue, Y. Liu, R. He, J. Mol. Catal. A: Chem. 259 (2006) 17.
- [10] F. Nipa Haque, A.J. Lough, R.H. Morris, *Inorg. Chim. Acta* 361 (2008) 3149.
- [11] P. Buskens, D. Giunta, W. Leitner, *Inorg. Chim. Acta* 357 (2004) 1969.
- [12] J. Bravo, J. Castro, S. Garcia-Fontana, M.C. Rodriguez-Martinez, G. Albertin, S. Antoniutti, A. Manera, *J. Organomet. Chem.* 692 (2007) 5481.
- [13] M. Chandra, A.N. Sahay, D.S. Pandey, M.C. Puerta, P. Valerga, *J. Organomet. Chem.* 648 (2002) 39.
- [14] A.K. Singh, P. Kumar, M. Yadav, D.S. Pandey, *J. Organomet. Chem.* 695 (2010) 567.
- [15] M. Arias, J. Concepción, I. Crivelli, A. Delgado, R. Díaz, A. Francois, F. Gajardo, R. López, A.M. Leiva, L. Loeb, *Chem. Phys.* 326 (2006) 54.
- [16] W. Henry, W.R. Browne, K.L. Ronayne, N.M. O'Boyle, J.G. Vos, J.J. McGarvey, *J. Mol. Struct.* 735–736 (2005) 123.
- [17] B.J. Coe, S.J. Glenwright, *Coord. Chem. Rev.* 203 (2000) 5.
- [18] J.G. Małecki, A. Maroń, *Polyhedron* 30 (2011) 1225.
- [19] J.G. Małecki, *Polyhedron* 30 (2011) 79.
- [20] J.G. Małecki, *Polyhedron* 29 (2010) 2489.
- [21] J.G. Małecki, R. Kruszyński, Z. Mazurak, *Polyhedron* 28 (2009) 3891.
- [22] J.G. Małecki, R. Kruszyński, Z. Mazurak, *J. Coord. Chem.* 61 (2008) 2186.
- [23] J.G. Małecki, R. Kruszyński, D. Tabak, J. Kusz, *Polyhedron* 26 (2007) 5120.
- [24] J.G. Małecki, R. Kruszyński, Z. Mazurak, *Polyhedron* 26 (2007) 4201.
- [25] J.G. Małecki, R. Kruszyński, *Polyhedron* 26 (2007) 2686.
- [26] J.G. Małecki, R. Kruszyński, *J. Coord. Chem.* 60 (2007) 2085.
- [27] N. Ahmad, J.J. Levinson, S.D. Robinson, M.F. Uttely, *Inorg. Synth.* 15 (1974) 48.
- [28] Gaussian 09, Revision A.1, M.J. Frisch, G.W. Trucks, H.B. Schlegel, G.E. Scuseria, M.A. Robb, J.R. Cheeseman, G. Scalmani, V. Barone, B. Mennucci, G.A. Petersson, H. Nakatsuji, M. Caricato, X. Li, H.P. Hratchian, A.F. Izmaylov, J. Bloino, G. Zheng, J.L. Sonnenberg, M. Hada, M. Ehara, K. Toyota, R. Fukuda, J. Hasegawa, M. Ishida, T. Nakajima, Y. Honda, O. Kitao, H. Nakai, T. Vreven, J.A. Montgomery, Jr., J.E. Peralta, F. Ogliaro, M. Bearpark, J.J. Heyd, E. Brothers, K.N. Kudin, V.N. Staroverov, R. Kobayashi, J. Normand, K. Raghavachari, A. Rendell, J.C. Burant, S.S. Iyengar, J. Tomasi, M. Cossi, N. Rega, J.M. Millam, M. Klene, J.E. Knox, J.B. Cross, V. Bakken, C. Adamo, J. Jaramillo, R. Gomperts, R.E. Stratmann, O. Yazyev, A.J. Austin, R. Cammi, C. Pomelli, J.W. Ochterski, R.L. Martin, K. Morokuma, V.G. Zakrzewski, G.A. Voth, P. Salvador, J.J. Dannenberg, S. Dapprich, A.D. Daniels, O. Farkas, J.B. Foresman, J.V. Ortiz, J. Cioslowski, and D.J. Fox, Gaussian, Inc., Wallingford CT, 2009.
- [29] A.D. Becke, *J. Chem. Phys.* 98 (1993) 5648.
- [30] C. Lee, W. Yang, R.G. Parr, *Phys. Rev. B* 37 (1988) 785.
- [31] K. Eichkorn, F. Weigend, O. Treutler, R. Ahlrichs, *Theor. Chim. Acc.* 97 (1997) 119.
- [32] M.E. Casida, in: J.M. Seminario (Ed.), *Recent Developments and Applications of Modern Density Functional Theory, Theoretical and Computational Chemistry*, vol. 4, Elsevier, Amsterdam, 1996, p. 391.
- [33] E. D. Glendening, A. E. Reed, J. E. Carpenter, and F. Weinhold, NBO (version 3.1).
- [34] N.M. O'Boyle, A.L. Tenderholt, K.M. Langner, *J. Comp. Chem.* 29 (2008) 839.
- [35] O.V. Dolomanov, L.J. Bourhis, R.J. Gildea, J.A.K. Howard, H. Puschmann, *J. Appl. Cryst.* 42 (2009) 339.
- [36] G.M. Sheldrick, *Acta Crystallogr., Sect. A64* (2008) 112.
- [37] G.R. Desiraju, T. Steiner, *The Weak Hydrogen Bond in Structural Chemistry and Biology*, Oxford University Press, 1999.
- [38] M. Trivedi, M. Chandra, D.S. Pandey, M.C. Puerta, P. Valerga, *J. Organomet. Chem.* 689 (2004) 879.
- [39] A. Romero, A. Vegas, A. Santos, *J. Organomet. Chem.* 310 (1986) C8.
- [40] J.G. Małecki, T. Groń, H. Duda, *Polyhedron* 31 (2012) 319.